Journal of Geophysical Research - Oceans

Supporting Information for

THE AGULHAS CURRENT TRANSPORTS SIGNALS OF LOCAL AND REMOTE INDIAN OCEAN NITROGEN CYCLING

Tanya A. Marshall[1], Daniel M. Sigman[2], Lisa M. Beal[3], Alan Foreman[4], Alfredo Martínez-García[4], Stéphane Blain[5], Ethan Campbell[6], François Fripiat[7], Robyn Granger[1], Eesaa Harris[1], Gerald H. Haug[3], Dario Marconi[2], Sergey Oleynik[2], Patrick A. Rafter[8], Raymond Roman[1], Kolisa Sinyanya[1], Sandi M. Smart[1,9], and Sarah E. Fawcett[1,10]

[1]Department of Oceanography, University of Cape Town, South Africa
[2]Department of Geosciences, Princeton University, USA
[3]Rosenstiel School of Marine and Atmospheric Science, University of Miami, USA
[4]Department of Climate Geochemistry, Max Planck Institute for Chemistry, Germany
[5]Laboratoire d'Océanographie Microbienne, Sorbonne Université, France
[6]School of Oceanography, University of Washington, USA
[7]Department of Geosciences, Environment and Society, Université Libre de Bruxelles, Belgium
[8]Department of Earth System Science, University of California, Irvine, USA
[9]Department of Geological Sciences, University of Alabama, USA
[10]Marine and Antarctic Research centre for Innovation and Sustainability (MARIS), University of Cape Town, South Africa

Contents of this file

Text S1 to S9
Figures S1 to S10
Tables S1 to S5

Introduction

The supporting information provides full details on methods, calculations, and uncertainty referenced in the main text, as well as figures and tables that support arguments made in the discussion section of the main text.

Text S1.

Correcting nitrate $\delta^{18}O$ for changes in salinity. During marine nitrification, the dominant source of the O atoms for nitrate is ambient seawater (Casciotti, et al., 2002; Casciotti, et al., 2010; Boshers, et al., 2019); changes in seawater $\delta^{18}O$ (i.e., $\delta^{18}O_{H2O}$) will thus affect the $\delta^{18}O$ of the nitrate that is produced. Generally, $\delta^{18}O_{H2O}$ varies little over the water column, but in regions characterised by large vertical salinity gradients, the measured $\delta^{18}O$ of nitrate may need to be corrected for changes in $\delta^{18}O_{H2O}$ (Knapp, et al., 2008; Fawcett, et al., 2015). This is because there exists a well-defined relationship between salinity and $\delta^{18}O_{H2O}$, with both parameters typically increasing towards the surface. The remineralization of organic matter in shallower waters where $\delta^{18}O_{H2O}$ is high could thus artefactually increase nitrate $\delta^{18}O$. In the subtropical Indian Ocean, $\delta^{18}O_{H2O}$ increases only slightly with decreasing depth (by 0.25‰ for a 0.42 rise in salinity between 0 and 500 m; Schmidt, G.A., G. R. Bigg and E. J. Rohling. 1999. "Global Seawater Oxygen-18 Database-v1.22"; https://data.giss.nasa.gov/o18data/). Applying a correction for salinity-driven depth variations in $\delta^{18}O_{H2O}$ following Knapp et al. (2008) decreases the nitrate $\delta^{18}O$ by an average of only 0.19‰ for our ASCA16 dataset (depth profiles of absolute salinity and the measured- and salinity-corrected nitrate $\delta^{18}O$ for the ASCA16 dataset are shown in Figure S4). Additionally, the error associated with the subtropical Indian Ocean $\delta^{18}O_{H2O}$/salinity relationship is considerable (r^2 =0.5, n=37). Finally, correcting nitrate $\delta^{18}O$ using coincidentally measured salinity assumes that all the nitrate was regenerated in situ (i.e., no preformed nitrate), which is not the case. We have thus chosen not to apply a salinity-based correction to our nitrate $\delta^{18}O$ dataset.

Text S2.

Identifying Red Sea Water in the Agulhas Current and adjacent recirculating waters. A Red Sea Water (RSW) lens is apparent in both the ASCA16 and SWINGS transects. RSW is typically most easily identified by its maxima in salinity and AOU relative to young and fresh Antarctic Intermediate Water (AAIW; see water mass labels on Figure 3 and S5) that occupies a similar density range (σ_θ = 27.0-27.4 kg.m^{-3}). The low purity of RSW in the Agulhas region, however, coupled with its interleaving with the surrounding water masses, dilutes the signal and makes identifying and quantifying RSW a challenge. Moreover, at the time of our sampling of the ASCA16 and SWINGS transects, RSW occurred coincident with (deeper) Upper Circumpolar Deep Water (UCDW; σ_θ = 27.4-27.7 kg.m^{-3}), which is also characterised by relative salinity and AOU maxima (Table 1 and Table S1 and S2 and Figure S5), further complicating the identification of RSW in Agulhas waters. RSW is, however, distinguishable from UCDW by its nitrate $\delta^{15}N$ and $\delta^{18}O$ that are 0.4-0.5‰ and 0.4‰, respectively, higher than the surrounding deep-water nitrate (Figure 4c and d inset and Figure S5b). The ASCA16 RSW lens is apparent as a nitrate-$\delta^{15}N$ maximum along the 27.45 kg.m^{-3} isopycnal (Figure 4c inset and S5b green-edged circles). These discrete data (n=5) are from offshore of the Agulhas Current core, between 34.1°S and 34.4°S and again at 34.7°S (Figure 5b). The SWINGS RSW lens is similarly apparent as a nitrate-$\delta^{15}N$ maximum between the 27.45 and 27.55 kg.m^{-3} isopycnals (Figure 4c inset and S5b green-edged pluses) and these discrete data (n=2) are also from offshore of the current core, at stations located at latitudes of 30.66°S; 32.15°E and 30.30°S; 32.80°E (Figure 1 and 4c).

Text S3.

The biogeochemistry of the southwest Indian Ocean in depth-space. All western boundary currents experience isopycnal shoaling at the position of the current, due to these currents maintaining geostrophic balance (Imawaki, et al., 2013). The water mass properties of such systems are therefore best viewed in density-space. By contrast, processes acting in the surface mixed layer are at times better viewed in depth-space since mixing can homogenize these waters and erode the density gradient across a broad depth interval. In other words, the density gradient across the surface mixed layer (i.e., surface to ~25.5 $kg.m^{-3}$ isopycnal) is narrow, sometimes only 0.1 $kg.m^{-3}$ over a 200 m depth interval, which condenses the data in density-space (for example, the subtropical waters in Figure 4). As such, we present the surface mixed layer data in both density (Figure 4) and depth space (Figure S6). The shallowest depth down to which surface conservative temperature, salinity, potential density, and nitrate concentrations are near-uniform approximates the depth of the mixed layer for each profile (white circles in Figure S1). Typically, mixed layer depth increases offshore, from as shallow as 29 m over the shelf to 220 m offshore.

Text S4.

Summertime nitrate isotope ratios in the Agulhas Current. A nearshore summertime transect of the Agulhas Current was sampled in January 2018 onboard the R/V *Nansen*. The transect covers only the seven most shoreward stations of the ASCA16 transect, from 33.34°S to 33.78°S (Figure S7). These data yield two major insights. First, across the transect, thermocline nitrate $\delta^{15}N$ is low, between 5‰ and 6‰ (Figure S7c). The $\delta^{15}N$ of thermocline nitrate in Tropical Thermocline Water (TTW) is slightly higher than in Subtropical Thermocline Water (STTW) (5.7‰ versus 5.3‰), as is the case for the ASCA16 and SWINGS datasets (Table 1, Figure 3b and 4c). The similarity of these data to our ASCA16 observations indicates that low-$\delta^{15}N$ nitrate is a perennial feature of the Agulhas Current thermocline and that STTW nitrate is consistently lower than TTW nitrate, as similarly demonstrated by the summer SWINGS dataset. Second, high AOU and nitrate concentrations over the shelf break in summer indicate that TTW has been vertically displaced (and compressed) to between 30 and 100 m from between 100 and 200 m where it is typically located (Figure S7a and b versus Figure 2a and b). The 26.4 $kg.m^{-3}$ isopycnal (the interface between the thermocline and Subantarctic Mode Water (SAMW); Table 1) is located at 270 m at the most offshore station (33.78°S) and rises to 52 m, the bottom depth at the shelf station (33.34°S). Along the bottom of the shelf and shelf break (33.46°S), nitrate $\Delta(15\text{-}18)$ is elevated to 3.4-3.5‰, while surface nitrate $\Delta(15\text{-}18)$ is lower, between -0.1 and 2.7‰. Together, these observations suggests that SAMW upwelled onto the shelf bottom but did not reach the surface to ventilate the shelf. The upwelling of these deeper waters likely explains the vertical displacement of TTW.

Text S5.

Estimating the magnitude of atmospheric nitrogen deposition to the greater Agulhas region. The $\delta^{15}N$ of fixed nitrogen (N) in the atmosphere is low, typically ranging between -14‰ and 2‰ (Altieri, et al., 2021). Atmospheric N deposition over the southwest Indian Ocean, if occurring at significant rates, could thus lower thermocline nitrate $\delta^{15}N$ and diminish the apparent role of N_2 fixation. The magnitude of the N deposition flux required to lower the Agulhas thermocline nitrate $\delta^{15}N$ from 6.9‰, as supplied by Subantarctic Mode Water, to the mean upper water column (σ_θ <26.7 $kg.m^{-3}$) value of 6.3‰ (also noting the minimum thermocline $\delta^{15}N$ of 4.2‰) is 3.0-12.8 Tg $N.a^{-1}$ (this range considers both the minimum and maximum atmospheric N isotope endmembers). This N deposition rate is estimated by first using a two-endmember mixing model to calculate the fraction of atmospheric N required to account for the entirety of the low-$\delta^{15}N$ thermocline nitrate in the greater Agulhas region, and then by multiplying this fraction by the water column-integrated nitrate burden. Additionally, we approximate the areal extent of the greater Agulhas region to be the highly retentive region of thermocline circulation enclosed by the 18 m dynamical height contour (black contour in Figure 1) of 7.3×10^{12} m^2 and assume a thermocline residence time of four years (i.e., as per the water volume flux estimate in Discussion 4.2.2). Our estimate of the N deposition rate required to lower thermocline nitrate $\delta^{15}N$ from the nitrate source value of 6.9‰ to the mean measured $\delta^{15}N$ of 6.3‰ represents the upper bound of atmospheric deposition. This is because the source waters to the greater Agulhas region likely contribute some amount of low-$\delta^{15}N$ nitrate along with low-nutrient surface waters, neither of which are accounted for by the N isotope mixing model outlined above, thus leading to an overestimation of the required atmospheric N deposition rate. It is nevertheless useful to compare our estimate of the upper bound to modelled N deposition rates.

The available modelled N deposition rates for the region range from 0.02 g $N.a^{-1}$ to 0.42 g $N.m^{-2}.a^{-1}$ and average 0.14 g $N.m^{-2}.a^{-1}$ (Somes, et al., 2016; Jickells, et al., 2017; Okin, et al., 2011), noting that the observational data required to initialize these models are sparse in the greater Agulhas region. This range of N deposition rates equates to an areal rate of 0.1-3.0 Tg $N.a^{-1}$ and a mean of 1.0 Tg $N.a^{-1}$ for the greater Agulhas region. Comparing the N deposition rate required to explain our isotope data to the modelled rates indicates that on average atmospheric N deposition to the greater Agulhas region is too low to account for the $\delta^{15}N$ of thermocline nitrate. This conclusion is consistent with the work of Grand et al. (2015c) that evaluated differences in the N:P ratio of the thermocline and aeolian dust (the latter typically characterized by a very high N:P ratio; (Baker, et al., 2010)) in the southwest Indian Ocean and concluded that the atmospheric deposition rate was far too low to account for the elevated subsurface N* observed in the western subtropical Indian Ocean.

Likewise, the terrestrial nitrogen flux from rivers and/or groundwater also appears to be negligible given the lack of any freshwater signal in our salinity data (Figure 3). Additionally, Russo et al. (2019) sampled the southeast African shelf extensively in both summer and winter and found evidence of freshwater input at only one of 38 shelf transects occupied in the summer. The authors attributed this signal to the Mzimvubu River and concluded that its influence penetrated <5 km offshore (i.e., not reaching the Agulhas Current) (Russo, et al., 2019). Moreover, even if there were a significant terrestrial nitrate flux to the Agulhas Current system, its magnitude will be small relative to the volume flux of the Agulhas Current, which transports ~77 $\times$ 10^6 cubic meters of water per second (Beal, et al., 2015). We thus conclude that terrestrial nitrate sourced from the southeast African coastline is highly unlikely to affect the biogeochemistry of the greater Agulhas region.

Text S6.

WOCE transects sampling the Agulhas region and its source waters. We use WOCE data to estimate the phosphorus (P) and nitrogen (N) fluxes in the greater Agulhas region (see Discussion 4.2.2 for details and Figure 1 for WOCE transect locations).

Text S6.1. **Tropical source waters**. For the topical source waters, we use the IO4 transect that samples zonally across the southern boundary of the Mozambique Channel along 24°S. Between 32°E and 38°E, a southward propagating Mozambique Channel eddy was sampled (Donohue & Toole, 2003), which represents the tropical source waters entering the greater Agulhas region. To estimate the tropical source water nutrient concentrations, we calculate the mean phosphate and nitrate concentrations over the upper 400 m from across the longitudes that sample the eddy.

Text S6.2. **Subtropical source waters.** For the subtropical source waters, we use the IO8 transect that samples meridionally across the eastern subtropical gyre along 95°E where the subtropical waters form and are therefore uninfluenced by the greater Agulhas region. To estimate the subtropical source water nutrient concentrations, we calculate the mean phosphate and nitrate concentrations over the upper 400 m from between 29°S and 36°S for the 2007 occupation. During the 2016 occupation of the IO8 transect, strong mesoscale anticyclonic eddies (with u-components of speed >0.4 $m.s^{-1}$) caused downwelling of low-nutrient surface waters to depth, which resulted in low mean nutrient concentrations that unlikely represent the mean condition (see GO-SHIP SADCP repository for details, https://currents.soest.hawaii.edu/go-ship/sadcp/cruises/2016_I08S/index.html). We therefore exclude the 2016 nutrient data from our analysis.

Text S6.3. **Greater Agulhas region waters.** For the greater Agulhas region waters, we use the IO6 transect that samples meridionally across the Agulhas Current and adjacent recirculating waters along ~30°E. To estimate the Agulhas water nutrient concentrations, we calculate the mean phosphate and nitrate concentrations from between 33°S and 38°S.

Text S7.

The $\delta^{15}N$ endmembers and their sensitivity to the N isotope equation in the one-box model. We use the available N isotope data (which are admittedly sparse) from across the South Indian Ocean to estimate the $\delta^{15}N$ of the endmembers that represent the sources and sinks to the upper (<400 m) greater Agulhas region (see Discussion 4.2.2 in the main text for details).

Text S7.1. **Tropical nitrate $\delta^{15}N$**. We set the nitrate $\delta^{15}N$ for the Tropical waters to the mean, concentration-weighted nitrate $\delta^{15}N$ measured over the upper 400 m of the IIOE2 transect (triangles in Figure 1), of 6.4 ± 0.7‰. As there are no measurements of nitrate $\delta^{15}N$ from elsewhere in the Mozambique Channel, we take our data as representative of the tropical waters that supply the Agulhas Current. We attribute the low $\delta^{15}N$ of this nitrate, relative to underlying Southeast Indian Subantarctic Mode Water (SEISAMW), to N_2 fixation likely occurring both in the channel and in northern tropical waters (i.e., north of the South Equatorial Current). Regardless of where the tropical N_2 fixation signal is generated, it must pass through the Mozambique Channel to enter the Agulhas Current.

Text S7.2. **Subtropical nitrate δ^{15}N.** We set the nitrate δ^{15}N for the Subtropical waters to the mean, concentration-weighted nitrate δ^{15}N measured over the 26.7-26.85 kg.m^{-3} isopycnal range, which represents SEISAMW in the southeast Indian Ocean (Lu, et al., 2021), of 7.0 ± 0.2‰. These data were collected during the 2016 occupation of IO8 (along ~95E; black, inverted triangles in Figure 1) when a mesoscale anticyclonic eddy greatly perturbed the upper 400 m of the water column, reaching down to 800 m. Downwelling and mixing of the low-nutrient (i.e., highly assimilated) surface waters with thermocline water resulted in an anomalously elevated nitrate δ^{15}N, of 7.9‰ (triangle symbols in Figure S8c; (Sigman & Fripiat, 2019)), that is unlikely to be representative of the mean condition (see S6.2). To resolve this, we set the subtropical nitrate δ^{15}N endmember to that of the underlying SEISAMW source that ultimately supplies nitrate to the surface and thermocline (Sarmiento, et al., 2004; Fripiat, et al., 2021).

Only one nitrate δ^{15}N profile exists between IO8 and the greater Agulhas region, along the pathway of the westward South Equatorial Current (15°S, 74°E, Figure 1; (Harms, et al., 2019)). Nitrate δ^{15}N from the South Equatorial Current profile and the eastern subtropical gyre profiles show no evidence of N_2 fixation (thermocline nitrate δ^{15}N is >7.0‰). With no available data between the South Equatorial Current and the South East Madagascar Current, we tentatively conclude that the Subtropical waters do not contribute low-δ^{15}N nitrate (i.e., via transport of a remote N_2 fixation signal) into the greater Agulhas region. Data from downstream of the Seychelles-Chagos island chain (i.e., between 50-70°E) would provide a better constraint on the subtropical nitrate δ^{15}N endmember supplied to the greater Agulhas region, but such data do not exist. Additional subtropical (20-27°S) nitrate δ^{15}N measurements from the center of the South Indian basin (black crosses in Figure 1; (Harms, et al., 2019)) are remarkably similar to the ASCA16 and SWINGS subtropical profiles and so are not considered source waters to the greater Agulhas region (see S7.3 below).

Text S7.3. Greater Agulhas nitrate δ^{15}N. We set the nitrate δ^{15}N for the Agulhas waters to the mean, concentration-weighted nitrate δ^{15}N measured over the upper 400 m of the ASCA16 transect (circles in Figure 1), of 6.0 ± 1.0‰. The subtropical profiles from the center of the South Indian basin sample between 20°S and 27°S along ~70°E (black crosses in Figure 1; (Harms, et al., 2019)). Here, Subtropical Thermocline Water (STTW) is characterised by a mean nitrate δ^{15}N of 5.2 ± 1.1‰ and AOU and nitrate concentration of 27.9 ± 10.5 μM and 1.6 ± 1.3 μM, respectively. These characteristics are similar to STTW sampled during the ASCA16 and SWINGS cruises (Table S1 and S2) and different from STTW in the eastern basin along IO8 (i.e., where nitrate δ^{15}N is >7.0‰; (Sigman & Fripiat, 2019); compare crosses and circles with inverted triangles in Figure S8c). The similar biogeochemical properties measured across the southwest Indian Ocean indicates that the subtropical profiles published by Harms, et al. (2019) cannot provide a source endmember to the greater Agulhas region (i.e., these stations are within the greater Agulhas region) and confirms the retention of subtropical waters in the western basin, extending to 70°E. Moreover, the contrast between eastern and western basin STTW nitrate δ^{15}N highlights basin-scale differences in N cycling.

Text S8.

Text S8.1. Calculating uncertainty on the volume, phosphorus, and nitrogen fluxes into and out of the greater Agulhas region. We use a one-box model to estimate the flux of newly-fixed nitrate into the greater Agulhas region (see Discussion 4.2.2). The uncertainty associated with the volume, phosphorus (P), and nitrogen (N) fluxes was calculated by propagating the uncertainty associated with the fluxes of water into and out of the greater Agulhas region and does not include uncertainty associated with the mean nutrient (phosphate and nitrate) concentrations. The volume, P, and N flux uncertainties are provided in Table S3. The mean and uncertainty associated with the organic P sinking flux is 5.3 ± 12.9 mmol.m^{-2}.a^{-1}, the organic N sinking flux is 95.4 ± 233.5 mmol.m^{-2}.a^{-1}, the N flux-based newly-fixed nitrate flux is 70.0 ± 84.7 mmol.m^{-2}.a^{-1}, and the N isotope flux-based newly-fixed nitrate flux is 238.7 ± 157.5 mmol.m^{-2}.a^{-1}. The uncertainties for the nutrient fluxes are propagated from the volume fluxes. This is because the nutrient concentrations are calculated as an average over the upper 400 m of the water column where the range in phosphate and nitrate concentrations is large.

Text S8.2. Sensitivity of the newly-fixed nitrate flux to the $\delta^{15}N$ of the endmembers. To assess the sensitivity of the newly-fixed nitrate flux to each of the $\delta^{15}N$ endmembers, we ran a sensitivity analysis using the standard deviation associated with each endmember. The results are provided in Table S4. The newly-fixed nitrate flux is most sensitive to the $\delta^{15}N$ of N_2 fixation, which is unsurprising given the relative magnitude of its uncertainty (of ± 1.0‰) relative to the mean value (of -1‰). The newly-fixed nitrate flux is also sensitive to the $\delta^{15}N$ of the greater Agulhas region, which also has a relatively large uncertainty (of 1.0‰) around the mean (of 6.0‰). Surprisingly, the newly-fixed nitrate flux is not particularly sensitive to the $\delta^{15}N$ assigned to sinking organic N, which gives us confidence in our choice of value.

Text S9.

Euphotic zone-integrated rates of N_2 fixation in the Agulhas Current and adjacent recirculating waters. We directly measured N_2 fixation rates throughout the euphotic zone at select stations across the Agulhas Current and adjacent recirculating waters in winter 2018 (ASCA18; near identical station locations to ASCA16; Figure 1). At three euphotic zone depths representing 55%, 10%, and 1% of the photosynthetically available radiation (PAR; measured during CTD down-casts using a PAR sensor), duplicate polycarbonate bottles were filled with 200 µm-prefiltered seawater for direct measurement of the N_2 fixation rate using the "dissolution method" (Mohr, et al., 2010; Klawonn, et al., 2015). Briefly, $^{15}N_2$ gas was added to gas-tight glass bottles that were completely filled with degassed (using helium) 0.2 µm-filtered seawater and agitated to ensure gas dissolution. This $^{15}N_2$-enriched seawater was added to the incubation bottles and an initial subsample was collected in a 20 mL glass vial closed with a gas-tight seal for analysis of $^{15}N_2$ atom % by membrane inlet mass spectrometry (White, et al., 2020). The N_2 fixation bottles were incubated on-deck for 24 hours in a custom-built incubator cooled with continuously running surface seawater and shaded with neutral density filters. Additional 1-L seawater samples were collected from each N_2 fixation depth (but not amended with $^{15}N_2$) and filtered immediately after collection through pre-combusted 0.3 µm glass fibre filters (GF-75s) for analysis of the initial $^{15}N/^{14}N$ ratio of the particulate organic N pool (White, et al., 2020).

The N_2 fixation experiments were terminated by filtration through a 0.3 µm GF-75 filter that was subsequently wrapped in pre-combusted foil and stored frozen at -80°C until analysis. Ashore, filters were oven dried for 24 hours at 45°C, then trimmed with a 20 mm metal punch to remove unused perimeter filter and folded into tin cups. Samples were analysed for PON content and $^{15}N/^{14}N$ using a Thermo Delta V Plus isotope ratio mass spectrometer interfaced with a Flash Elemental Analyser 1112 Series. The volumetric rates of N_2 fixation (nmol L^{-1} d^{-1}) were calculated following (Montoya, et al., 1996), taking into account the initial $^{15}N/^{14}N$ of the PON pool and the measured fractional ^{15}N enrichment of the seawater N_2 at the start of the experiments (White, et al., 2020). The euphotic zone-integrated N_2 fixation rates, computed by integrating between the 55% and 1% PAR rate measurements (with the base of the euphotic zone defined as the penetration depth of 1% of surface PAR (Kirk, 1994)) range from 27.8 to 236.1 µmol $N.m^{-2}.d^{-1}$ (Table S5).

Supplementary figures 1-10

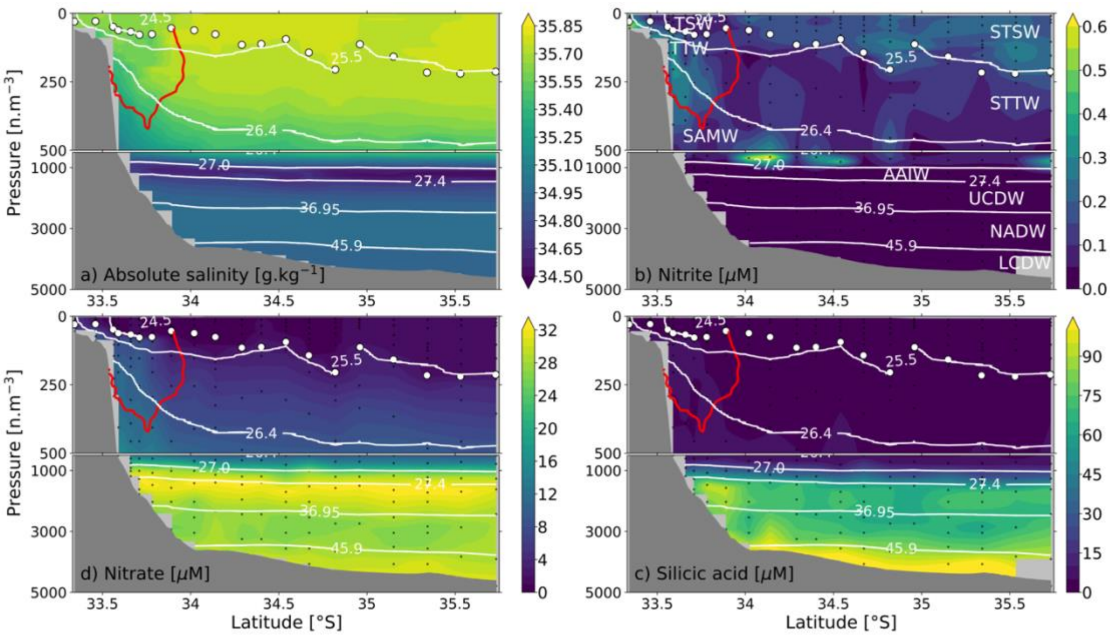

Figure S1. **Full depth nutrient concentrations across the ASCA16 transect**. Gridded section plots from the ASCA16 transect of **a**) absolute salinity [g.kg^{-1}] and **b**) nitrite, **c**) nitrate, and **d**) silicic acid concentrations [μM]. The red contour depicts the 1 m.s^{-1} along-stream current speed, indicating the position of the Agulhas Current core at the time of sampling, and the white contours show the isopycnal boundaries of the water masses along σ_θ, σ_2, and σ_4 (see Table 1). The white circles indicate the depth of the mixed layer at each station and the small black circles show discrete sampling depths. The y-axis of each plot is non-linear to focus on the upper 500 m while still showing the full depth concentrations. TSW: Tropical Surface Water; STSW: Subtropical Surface Water; TTW: Tropical Thermocline Water; STTW: Subtropical Thermocline Water; SAMW: Subantarctic Mode Water; AAIW: Antarctic Intermediate Water; UCDW: Upper Circumpolar Deep Water; NADW: North Atlantic Deep Water; LCDW: Lower Circumpolar Deep Water.

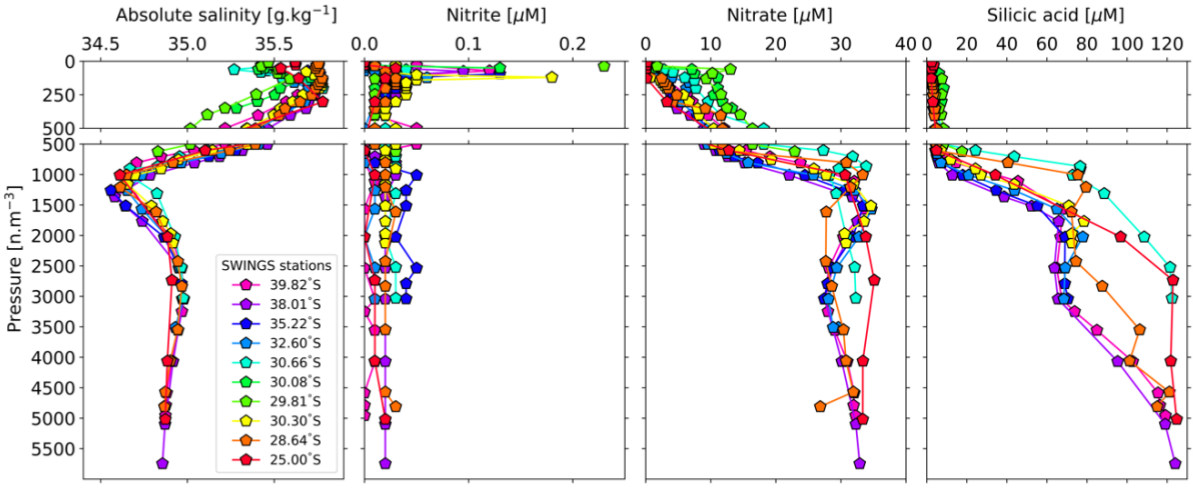

Figure S2. **Full depth profiles of nutrient concentrations across the SWINGS transect**. Discrete depth profiles of **a**) absolute salinity [g.kg^{-1}] and **b**) nitrite, **c**) nitrate, and **d**) silicic acid concentrations [µM] for samples collected during the SWINGS cruise. The legend provides station latitude. Note that the depth (i.e., pressure) axis is shown at two resolutions, with the top panels showing the surface-to-thermocline data and the bottom panels showing the deep-water data.

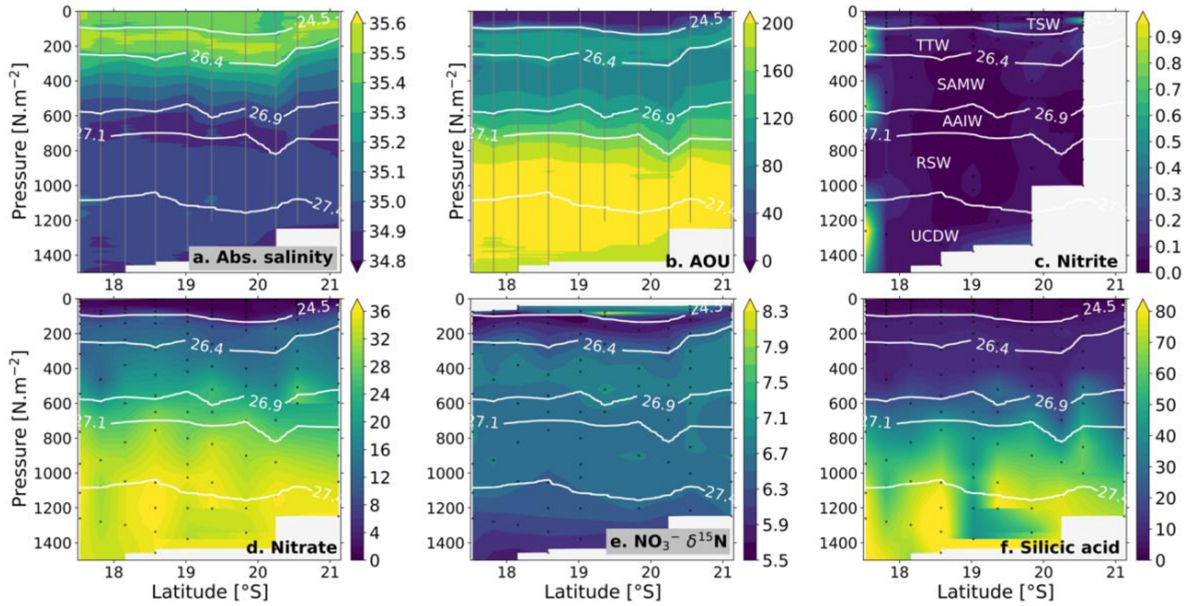

Figure S3. **Biogeochemistry of the western Mozambique Channel.** Gridded section plots from the IIOE2 transect of **a**) absolute salinity [g.kg^{-1}], **b**) apparent oxygen utilization (AOU) [µM], **c**) nitrite concentration [µM], **d**) nitrate concentration [µM], **e**) nitrate δ^{15}N [‰], and **f**) silicic acid concentration [µM]. White contours indicate the isopycnal boundaries of water masses (see Table 2) and small black circles indicate discrete sampling depths. Water mass abbreviations are as in Figure S1 and include RSW: Red Sea Water.

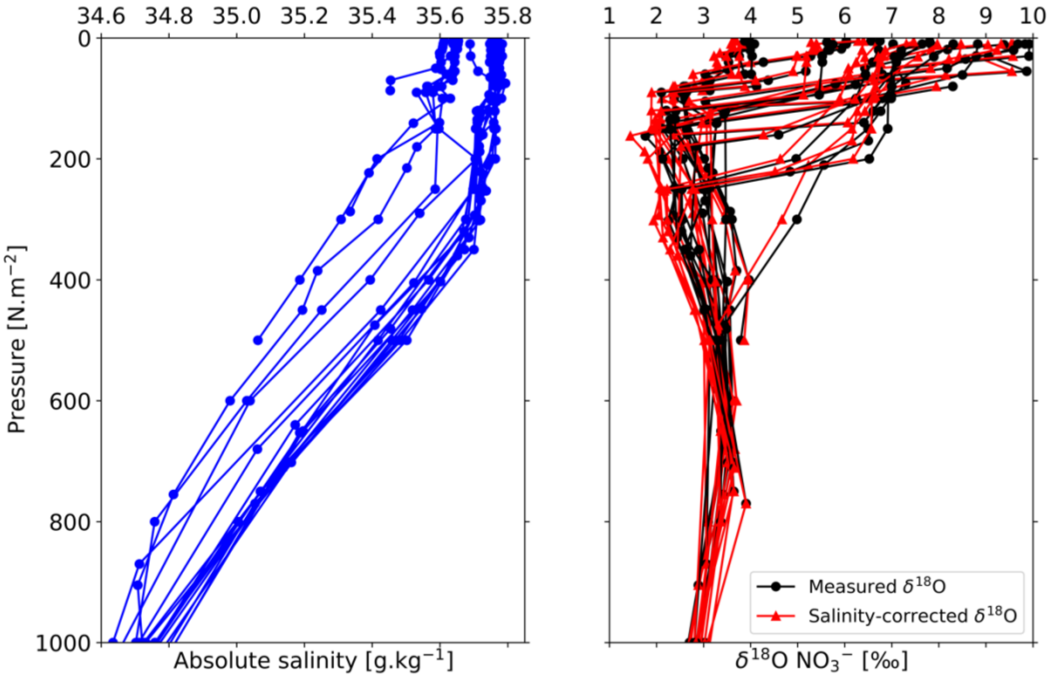

Figure S4. Depth profiles of a) absolute salinity [g.kg^{-1}] and b) nitrate δ^{18}O [‰] from across the Agulhas Current and adjacent recirculating waters. In panel **b**, the black profiles show the measured nitrate δ^{18}O data and the red profiles show the salinity-corrected nitrate δ^{18}O data. This exercise reveals that correcting for salinity-driven changes in $\delta^{18}O_{H2O}$ makes almost no difference to the δ^{18}O of nitrate.

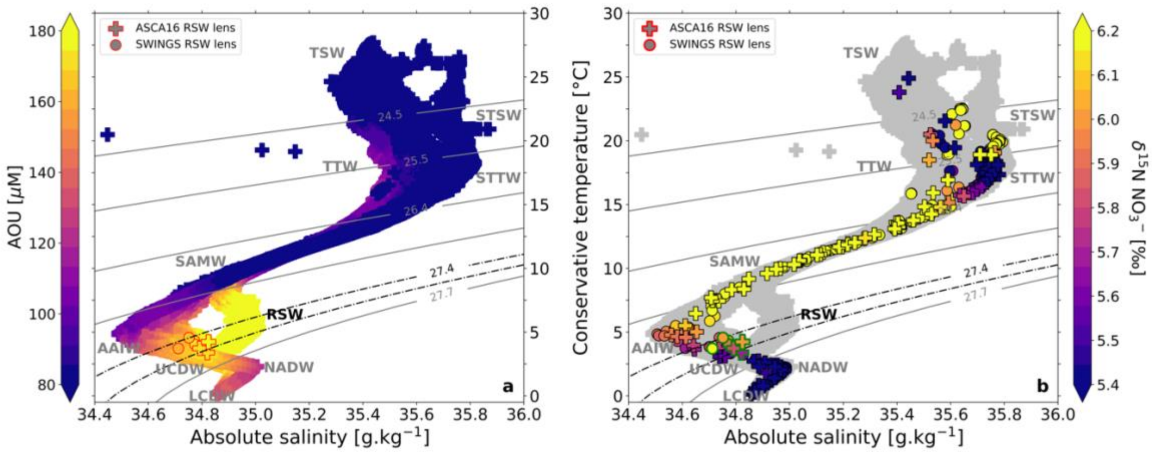

Figure S5. Conservative temperature [°C] versus absolute salinity [g.kg^{-1}] for the ASCA16 (circle symbols), IIEO2 (triangle symbols), and SWINGS (plus symbols) datasets. Symbol colours indicate **a**) apparent oxygen utilisation (AOU) [μM] and **b**) nitrate δ^{15}N [‰]. The symbols outlined in red (on panel **a**) and green (on panel **b**) show discrete samples representing the Red Sea Water (RSW) lenses, as per the legend. In panel **b**, all discrete ASCA16 and SWINGS isotope samples are outlined in black while the underlying grey symbols show the high-resolution CTDO data (including from the IIEO2 cruise, see Figure 3). Black and grey contours indicate the potential density anomalies (in kg.m^{-3}) that form the boundaries between water masses (see Table 1). TSW: Tropical Surface Water; STSW: Subtropical Surface Water; TTW: Tropical Thermocline Water; STTW: Subtropical Thermocline Water; SAMW: Subantarctic Mode Water; AAIW: Antarctic Intermediate Water; RSW: Red Sea Water; UCDW: Upper Circumpolar Deep Water; NADW: North Atlantic Deep Water; IDW: Indian Deep Water; LCDW: Lower Circumpolar Deep Water.

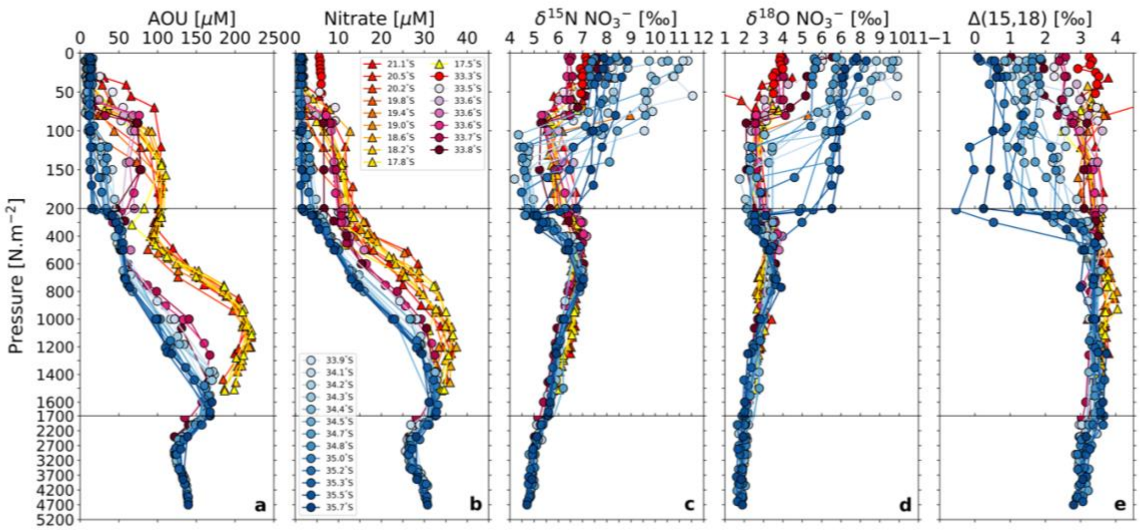

Figure S6. Full depth profiles of **a**) apparent oxygen utilization (AOU) [μM], **b**) nitrate concentration [μM], **c**) nitrate $\delta^{15}N$ [‰], **d**) nitrate $\delta^{18}O$ [‰], and **e**) nitrate Δ(15-18) [‰] from ASCA16 (circles) and IIEO2 (triangles). The legend provides station latitude. The depth (i.e., pressure) axis is shown at three resolutions to separate the surface, thermocline, and deep waters.

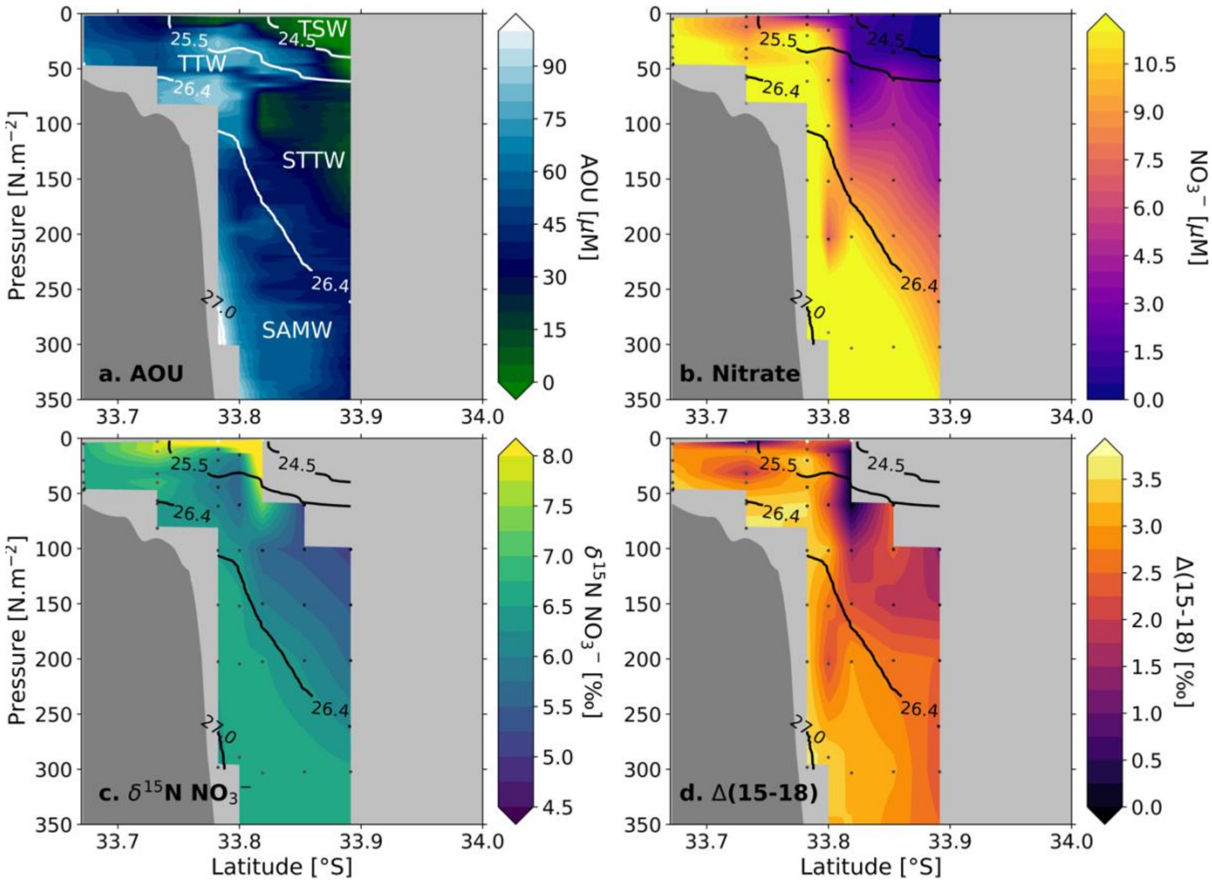

Figure S7. Summertime biogeochemistry across the Agulhas Current. Gridded section plots from the nearshore ASCA 2018 summer transect of **a)** apparent oxygen utilization (AOU) [μM], **b)** nitrate concentration [μM], **c)** nitrate δ^{15}N [‰], and **d)** nitrate Δ(15-18). Black and white contours indicate the isopycnal boundaries of the water masses (Table 1). Dark grey points indicate the discrete sampling depths.

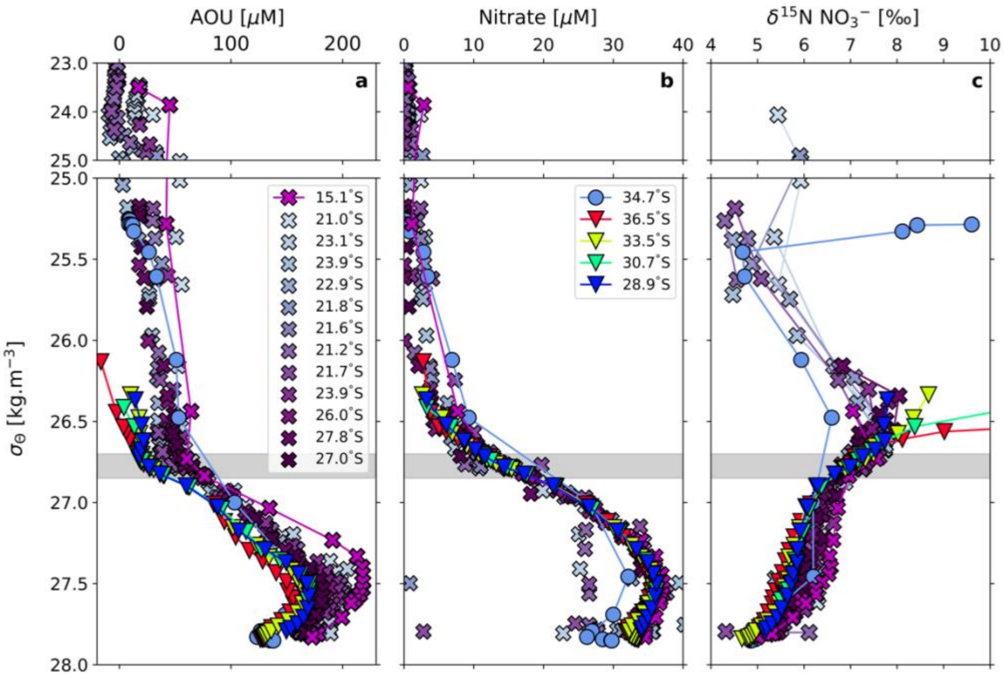

Figure S8. Density profiles of **a)** apparent oxygen utilisation (AOU) [μM], **b)** nitrate concentration [μM], and **c)** nitrate $\delta^{15}N$ [‰] for samples collected in the eastern, northern, and central South Indian Ocean (see Figure 1 for sampling locations). Triangles indicate profiles sampled along 95°E during a WOCE IO8S cruise (Sigman & Fripiat, 2019) and crosses show profiles collected at ~74°E during the MSM-59/2 and SO-259 cruises (Harms, et al., 2019). The light-blue circles show a typical subtropical profile from the greater Agulhas region, included to highlight the difference between the eastern and western basin profiles. Profile latitude is provided in the legend. The y-axis is segmented to highlight the thermocline (σ_θ = 25.0-26.4 kg.m^{-3}). The grey shading indicates the isopycnal range used to calculate the mean properties of Southeast Indian Subantarctic Mode Water (see S7.2). For the eastern basin profiles, no nitrate $\delta^{15}N$ data are available for σ_θ <26.2 kg.m^{-3} where the nitrate concentration is <2.65 μM.

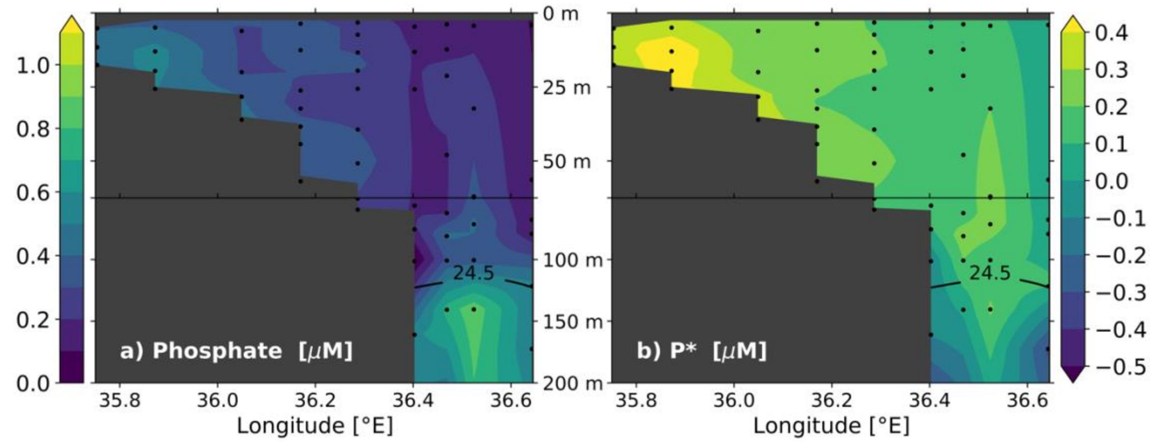

Figure S9. Phosphate and P* concentrations on the western Mozambique Channel shelf. Gridded section plots of a zonal (cross-shelf) transect sampled during the IIEO2 cruise showing **a)** phosphate concentration [μM] and **b)** P* (=[PO_4^{3-}] – [NO_3^-] ÷ 16; (Deutsch, et al., 2007)) [μM]. The y-axis in nonlinear to highlight the shelf concentrations. The black contour indicates the 24.5 kg.m^{-3} isopycnal boundary that separates Tropical Surface Water (above) and Tropical Thermocline Water (below). Dark grey points indicate the discrete sampling depths. Nutrient samples were collected as per those from the Mozambique Channel meridional transect described in Methods 2.2 of the main text. Phosphate and nitrate concentrations were measured at the Marine Biogeochemistry Lab at the University of Cape Town (UCT-MBL). Nitrate concentrations were measured using a Lachet QuickChem® Flow Injection Analysis platform with a precision of 0.2 μM and detection limit of 0.12 μM (Grasshoff, et al., 1999). Phosphate concentrations were measured manually using standard colourimetric methods (Grasshoff, et al., 1999; Strickland & Parsons, 1972) and a Genesys 30 Visible spectrophotometer, with a precision of 0.1 μM and a detection limit of 0.05 μM. Aliquots of a certified reference material (JAMSTEC) were included in each autoanalyzer and manual run to ensure measurement accuracy.

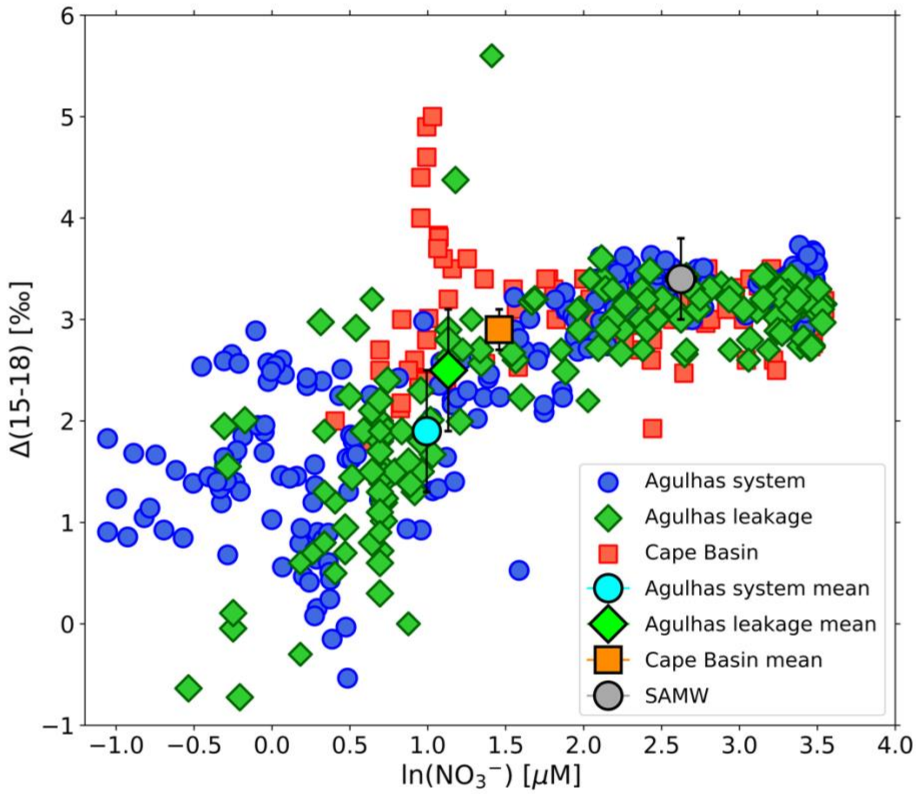

Figure S10. The Δ(15-18) of nitrate in the greater Agulhas region, Agulhas leakage, and background Cape Basin. Nitrate Δ(15-18) [‰] vs ln([NO_3^-]) [μM] for the ASCA16 and Cape Basin data. Symbol colour and shape indicate the sampling region. The mean ln([NO_3^-]) and concentration-weighted nitrate Δ(15-18) values for each region (for σ_θ <26.4 kg.m^{-3}) are shown in a lighter shade and outlined in black. The bold grey circle outlined in black shows the mean ln([NO_3^-]) and concentration-weighted nitrate Δ(15-18) measured for Subantarctic Mode Water (SAMW). The data from the Cape Basin are detailed in Figure 8. Figure S10 clearly shows that shallow nitrate in Agulhas leakage retains much of the low-Δ(15-18) signal that is characteristic of the greater Agulhas region even as it mixes with generally higher-Δ(15-18) Cape Basin nitrate.

Supplementary tables 1-5

Table S1. Mean values (± 1 SD) of absolute salinity [g.kg^{-1}], conservative temperature [°C], oxygen concentration [uM], apparent oxygen utilization (AOU) [µM], silicic acid, nitrite, and nitrate concentrations [µM], and concentration-weighted nitrate δ^{15}N [‰], δ^{18}O [‰], and Δ(15-18) [‰] for the water masses identified in the ASCA16 dataset. Water masses are defined by potential density anomalies, σ_θ [kg.m^{-3}], and their core properties are listed in brackets. The narrow density range between the surface and thermocline condenses the shallow data in density-space (S3); we thus report surface and thermocline water mass properties averaged over depth rather than density. The row subheadings *Tropical* and *Subtropical* refer to inshore and offshore of the Agulhas Current core, respectively. The two most coastal ASCA16 stations (33.34°S and 33.46°S) are excluded from the inshore mean as they are both influenced by upwelling.

Table S2. Mean values (± 1 SD) of absolute salinity [g.kg^{-1}], conservative temperature [°C], oxygen concentration [uM], apparent oxygen utilization (AOU) [µM], silicic acid, nitrite, and nitrate concentrations [µM], and concentration-weighted nitrate δ^{15}N [‰] for the water masses identified in the SWINGS dataset. Water masses are defined by potential density anomalies, σ_θ [kg.m^{-3}], and their core properties are listed in brackets. The narrow density range between the surface and thermocline condenses the shallow data in density-space (S3); we thus report surface and thermocline water mass properties averaged over depth rather than density. The row subheadings *Tropical* and *Subtropical* refer to inshore and offshore of the Agulhas Current core, respectively. There are no nitrate δ^{18}O measurements (and thus no Δ(15-18)) available for the SWINGS dataset.

Table S1

Water mass		**Abbrev**	**Potential density, σ_0 [kg.m^{-3}]**	**Absolute salinity [g.kg^{-1}]**	**Conservative temperature, θ [°C]**	**Oxygen [µM]**	**AOU [µM]**	**$Si(OH)_4$ [µM]**	**NO_2^- [µM]**	**NO_3^- [µM]**	**$\delta^{15}N$ NO_3^- [‰]**	**$\delta^{18}O$ NO_3^- [‰]**	**Δ(15-18) [‰]**
Tropical	Tropical Surface Water	TSW	<24.5	35.6 ± 0.54 (35.6 ± 0.49)	22.5 ±0.07 (22.2 ± 0.68)	201.8 ± 2.4 (198.3 ± 10.4)	12.8 ±2.5 (17.3 ± 12.6)	2.6 ± 0.3 (2.7 ± 0.3)	0.1 ± 0.0 (0.1 ± 0.0)	0.8 ± 0.4 (1.1 ± 0.9)	6.7 ± 0.3 (6.5 ± 1.2)	4.4 ± 0.4 (4.0 ± 1.2)	2.3 ± 0.3 (2.5 ± 1.2)
Tropical	Tropical Thermocline Water	TTW	24.5 - 26.4	35.6 ±0.04 (35.6 ± 0.03)	16.9 ± 2.10 (17.2 ± 1.82)	172.5 ± 18.5 (162.7± 14.3)	65.5 ± 16.4 (73.9 ± 14.3)	5.5 ± 1.4 (5.6 ± 1.4)	0.2 ± 0.1 (0.2 ±0.1)	8.0 ± 2.1 (7.8 ± 1.8)	6.0 ± 0.3 (5.8 ± 0.3)	2.7 ± 0.4 (2.7 ± 0.4)	3.2 ± 0.3 (3.2 ± 0.3)
Subtropical	Subtropical Surface Water	STSW	24.5 - 25.5	35.8 ±0.25 (35.8 ± 0.05)	19.5 ± 2.17 (19.7 ± 1.59)	213.0 ± 21.8 (214.4 ± 1.8)	13.2 ± 27.2 (11.1 ± 2.7)	2.7 ± 0.5 (2.6 ± 0.4)	0.2 ± 0.1 (0.2 ± 0.0)	1.2 ± 0.6 (1.0 ± 0.5)	7.2 ± 0.7 (8.0 ± 0.7)	5.9 ± 0.7 (6.7 ± 0.7)	1.3 ± 0.9 (1.3 ± 0.8)
Subtropical	Subtropical Thermocline Water	STTW	25.5 - 26.4	35.7 ± 0.17 (35.7 ± 0.02)	16.5 ± 2.04 (18.4 ± 0.77)	198.7 ± 10.5 (201.8 ± 9.0)	45.8 ± 8.8 (29.9 ± 11.9)	4.1 ± 0.6 (3.3 ± 0.6)	0.1 ± 0.0 (0.1 ± 0.1)	5.9 ± 1.9 (3.0 ± 1.4)	5.7 ± 0.5 (4.9 ± 0.7)	3.0 ± 0.5 (2.8 ± 0.8)	2.7 ± 0.5 (2.1 ± 0.8)
Subantarctic Mode Water		SAMW	26.4 - 27.0	35.1 ± 0.23 (35.1 ± 0.06)	35.1 ± 0.23 (35.1 ± 0.06)	11.1 ± 1.86 (11.3 ± 0.38)	203.5 ± 6.7 (209.3 ± 2.5)	65.3 ± 15.7 (57.7 ± 3.6)	9.9 ± 5.6 (6.9 ± 2.3)	0.1 ± 0.13 (0.2 ± 0.15)	15.2 ± 4.3 (13.8 ± 1.1)	6.7 ± 0.4 (6.9 ± 0.1)	3.3 ± 0.4 (3.5 ± 0.1)
Antarctic Intermediate Water		AAIW	27.0 - 27.4	35.1 ± 0.23 (35.1 ± 0.06)	11.1 ± 1.86 (11.3 ± 0.38)	203.5 ± 6.7 (209.3 ± 2.5)	65.3 ± 15.7 (57.7 ± 3.6)	9.9 ± 5.6 (6.9 ± 2.3)	0.1 ± 0.1 (0.2 ± 0.2)	15.2 ± 4.3 (13.8 ± 1.1)	6.7 ± 0.4 (6.9 ± 0.1)	3.3 ± 0.4 (3.5 ± 0.1)	3.4 ± 0.4 (3.4 ± 0.1)
Red Sea Water lenses		RSW	27.45 - 27.55	34.6 ± 0.06 (34.6 ± 0.06)	5.4 ± 1.05 (5.3 ± 0.63)	178.3 ± 14.1 (181.3 ± 12.4)	128.0 ± 18.2 (125.8 ± 12.0)	38.3 ± 11.3 (36.9 ± 6.6)	0.0 ± 0.0 (0.0 ± 0.0)	28.3 ± 2.4 (28.6 ± 1.3)	6.0 ± 0.1 (6.0 ± 0.1)	2.6 ± 0.1 (2.6 ± 0.1)	3.4 ± 0.1 (3.4 ± 0.1)
Upper Circumpolar Deep Water		UCDW	27.4 - σ_2 =36.9	34.7 ± 0.03	4.2 ± 0.25	151.0 ± 6.9	164.3 ± 5.2	63.9 ± 2.2	0.0 ± 0.0	32.2 ± 0.3	6.0 ± 0.0	2.6 ± 0.1	3.4 ± 0.0
North Atlantic Deep Water		NADW	σ_2=36.9 - σ_4 = 45.9	35.0 ± 0.02 (35.0 ± 0.00)	2.1 ± 0.31 (2.1 ± 0.14)	202.7 ± 8.1 (207.3 ± 2.6)	128.6 ± 6.3 (124.2 ± 1.9)	75.0 ± 8.1 (72.8 ± 6.6)	0 ±0.00	27.4 ± 0.8 (27.0 ± 0.7)	5.0 ± 0.0 (5.0 ±0.0)	1.9 ± 0.1 (1.9 ± 0.1)	3.1 ± 0.1 (3.1 ± 0.1)
Lower Circumpolar Deep Water		LCDW	σ_4 > 45.9	34.9 ± 0.01 (34.9 ± 0.01)	1.0 ± 0.2 (0.9 ± 0.09)	206.2 ±1.1 (205.7 ± 0.8)	134.5 ± 2.5 (136.5 ± 1.3)	98.8 ± 7.1 (105.5 ± 3.6)	0 ±0.00	29.3 ± 0.8 (30.0 ± 0.4)	4.9 ± 0.0 (4.8 ± 0.0)	1.8 ± 0.1 (1.8 ± 0.1)	3.0 ± 0.0 (3.0 ± 0.0)

Table S2

Water mass		Abbrev	Potential density, σ_θ [kg.m^{-3}]	Absolute salinity [g.kg^{-1}]	Conservative temperature, θ [°C]	Oxygen [µM]	AOU [µM]	$Si(OH)_4$ [µM]	NO_2^- [µM]	NO_3^- [µM]	$\delta^{15}N$ NO_3^- [‰]
Tropical	Tropical Surface Water	TSW	<24.5	35.4 ± 0.05 (35.5 ± 0.06)	25.7 ± 1.76 (27.0 ± 0.59)	203.6 ± 24.0 (195.6 ± 28.4)	14.8 ± 26.0 (5.3± 2.5)	2.4 ± 1.0 (1.7 ± 0.1)	0.1 ± 0.07 (0.0 ± 0.01)	3.9 ± 3.1 (0.2 ± 0.1)	5.6 ± 0.0 (NAN)
	Tropical Thermocline Water	TTW	24.5 - 26.4	35.5 ±0.06 (35.5 ± 0.07)	16.9 ± 2.30 (17.7 ± 2.94)	214.6 ± 6.5 (215.7 ± 6.4)	78.1 ± 26.1 (72.5 ± 19.3)	3.8 ± 0.9 (6.5 ± 1.5)	0.0 ± 0.4 (0.0 ± 0.06)	10.5 ± 1.0 (9.6 ± 2.5)	6.3 ± 0.3 (6.2 ± 0.4)
Subtropical	Subtropical Surface Water	STSW	24.5 - 25.5	35.7 ±0.04 (35.7 ± 0.22)	20.5 ± 0.92 (22.0 ± 2.55)	204.1 ± 29.0 (203.2 ± 30.6)	11.5 ± 16.0 (6.0 ± 16.4)	2.0 ± 0.4 (2.0 ± 0.5)	0.0 ± 0.04 (0.0 ± 0.03)	0.6 ± 0.6 (0.4 ± 0.6)	5.8 ± 0.7 (6.0 ± 1.9)
	Subtropical Thermocline Water	STTW	25.5 - 26.4	35.7 ± 0.08 (35.7 ± 0.04)	16.5 ± 1.23 (18.1 ± 1.60)	192.1 ± 21.9 (188.9 ± 31.0)	32.7 ± 9.2 (24.7 ± 7.4)	3.4 ± 0.5 (3.0 ± 0.5)	0.0 ± 0.02 (0.0 ± 0.02)	5.0 ± 2.0 (3.0 ± 1.4)	5.8 ± 0.6 (5.1 ± 0.7)
Subantarctic Mode Water		SAMW	26.4 - 27.0	35.1 ± 0.23 (35.1 ± 0.06)	10.9 ± 1.84 (11.3 ± 0.37)	203.9 ± 12.8 (207.8 ± 8.9)	65.7 ± 18.2 (57.1 ± 6.6)	12.3 ± 12.9 (8.6 ± 5.9)	0.0 ± 0.01 (0.0 ± 0.01)	16.9 ± 6.5 (15.3 ± 3.9)	6.6 ± 0.5 (6.7 ± 0.4)
Antarctic Intermediate Water		AAIW	27.0 - 27.4	34.7 ± 0.06 (34.6 ± 0.06)	5.5 ± 1.10 (5.4 ± 0.59)	176.4 ± 16.9 (176.7 ± 15.1)	129.7 ± 17.3 (127.0 ± 12.0)	47.0 ± 18.5 (45.8 ± 17.1)	0.0 ± 0.01	30.3 ± 2.4 (30.4 ± 1.5)	6.0 ± 0.1 (6.0 ± 0.1)
Red Sea Water lenses		RSW	27.45 - 27.55	34.8 ± 0.03	3.9 ± 0.25	148.6 ± 11.9	172.4 ± 7.5	81.0 ± 10.8	0.0 ± 0.00	31.6 ± 2.4	5.9 ± 0.1
Upper Circumpolar Deep Water		UCDW	27.4 - σ_2 =36.9	34.8 ± 0.07 (34.8 ± 0.06)	3.1 ± 0.48 (3.2 ± 0.46)	167.3 ± 11.8 (165.4 ± 11.4)	160.0 ± 8.8 (162.2 ± 7.6)	72.8 ± 11.3 (72.5 ± 11.3)	0.0 ± 0.01	31.5 ± 2.0 (31.7 ± 2.0)	5.5 ± 0.1 (5.6 ± 0.1)
Indian Deep Water		IDW	*27.45 - σ_4 = 45.9*	34.9 ± 0.00	1.8 ± 0.04	211.9 ± 0.29	177.3 ± 0.4	122.7 ± 0.3	0.0 ± 0.00	35 ± 0.1	5.4 ± 0.1
North Atlantic Deep Water		NADW	σ_2=36.9 - σ_4 = 45.9	35.0 ± 0.02 (35.0 ± 0.0)	2.1 ± 0.30 (2.0 ± 0.14)	200.7 ± 9.2 (204.9 ± 4.1)	130.7 ± 7.3 (126.7 ± 4.3)	81.3 ± 18.2 (81.0 ± 19.2)	0.0 ± 0.01	29.1 ± 1.4 (28.8 ± 1.5)	5.1 ± 0.1 (5.1 ± 0.1)
Lower Circumpolar Deep Water		LCDW	σ_4 > 45.9	34.9 ± 0.01 (34.9 ± 0.01)	0.7 ± 0.34 (0.5 ± 0.21)	210.2 ± 2.0 (210.5 ± 2.0)	133.4 ± 3.0 (134.6 ± 2.4)	106.0 ± 9.1 (110.0 ± 6.6)	0.0 ± 0.01	30.9 ± 1.0 (31.2 ± 0.9)	4.9 ± 0.0 (4.9 ± 0.0)

Table S3. Uncertainty associated with the volume and nutrient fluxes into the greater Agulhas region from the one-box model used to estimate the newly-fixed nitrate flux. Uncertainty is derived through error propagation of the relative volume contributions to the Agulhas Current ± their respective uncertainties (see Discussion 4.2.2 for details).

Box model inputs	Tropical source waters	Subtropical source waters
Volume fluxes [Sv]	6.2 ± 1.4	17.0 ± 4.9
Phosphate fluxes [mmol.m^{-2}.a^{-1}]	16.1 ± 3.6	43.2 ± 12.4
Nitrate fluxes [mmol.m^{-2}.a^{-1}]	187.6 ± 42.0	497.8 ± 142.8

Table S4. Sensitivity of the newly-fixed nitrate flux [mmol.m^{-2}.a^{-1}] to the $\delta^{15}N$ of the endmembers [‰] used in the nitrogen isotope equation. Each endmember was tested using ± 1 standard deviation around the mean (see S8.2 for details).

$\delta^{15}N$ endmember	Tropical	Subtropical	Agulhas	Sinking	N_2 fixation	Newly-fixed nitrate flux
This study	6.4	7.0	6	5.1	-1	238.7
Tropical	6.4 - 0.7	7	6	5.1	-1	107.4
Tropical	6.4 + 0.7	7	6	5.1	-1	370.0
Subtropical	6.4	7.0 - 0.2	6	5.1	-1	139.1
Subtropical	6.4	7.0 + 0.2	6	5.1	-1	388.2
Agulhas	6.4	7	6.0 - 1.0	5.1	-1	898.7
Agulhas	6.4	7	6.0 + 1.0	5.1	-1	-421.3
Sinking	6.4	7	6	5.1 - 0.7	-1	305.4
Sinking	6.4	7	6	5.1 + 0.7	-1	171.9
N_2 fixation	6.4	7	6	5.1	-1 - 1	119.3
N_2 fixation	6.4	7	6	5.1	-1 + 1	2386.7

Table S5. Euphotic zone-integrated N_2 fixation rates measured across the ASCA transect in winter 2018 (see S9 for details)**.**

Latitude	Longitude	Euphotic zone depth [m]	N_2 fixation rate [μmol N.m^{-2}.d^{-1}]
33.33°S	27.59°E	20	30.8
33.37°S	27.37°E	20	27.8
33.55°S	27.49°E	45	34.9
33.54°S	27.47°E	80	113.8
35.15°S	28.37°E	80	170.5
34.24°S	28.06°E	70	236.1
34.59°S	28.26°E	120	204.8
35.44°S	28.54°E	120	155.7